isardSAT®

Sentinel-3 For Science-SAR Altimetry Studies- Study 2: SCOOP

-SAR Level-2: Algorithms Technical Baseline Document (ATBD)-

isardSAT Reference: ISARD_ESA_SCOOP_ATBD_758
Issue: 1.a

Prepared by: Eduard Makhoul
Reviewed by: Mònica Roca
Approved by: Mònica Roca
4 February 2019

Change Record

Date	Issue	Section	Comment
4 February 2019	1.a	all	First formal issue

Control Document

Process	Name	Date
Written by:	Eduard Makhoul	4 February 2019
Reviewed by:	Mònica Roca	4 February 2019
Approved by:	Mònica Roca	4 February 2019

Distribution List

Company	Name
ESA	Jérôme Nemeviste Marco Restano Americo Ambrozio
isardSAT	Eduard Makhoul Mònica Roca Roger Escolà
SatOC	David Cotton Ellis Ash
NOC	Christine Gommenginger Chris Banks Clare Bellingham Francisco Mir Calafat Helen Snaith
CLS	Moreau Thomas Matthias Raynal
Noveltis	Eric Jeansou Mathilde Cancet
TUDa/Bonn	Luciana Fenoglio
TUDelft	Marc Naeije
University Porto	Joana Fernandes Clara Lázaro

Contents

Change Record iii

Control Document iii

Distribution List iii

List of Figures vii

Nomenclature x

1 Introduction 1
- 1.1 Document Organisation . . . 2
- 1.2 Acronyms . . . 2
- 1.3 References . . . 3
  - 1.3.1 Applicable Documents . . . 3
  - 1.3.2 Reference Documents . . . 3

2 SAR Ocean retracker 5
- 2.1 General overview . . . 6
- 2.2 Pre-processing . . . 7
  - 2.2.1 Purpose and scope . . . 7
  - 2.2.2 Data block and Diagram . . . 7
  - 2.2.3 Mathematical Description . . . 7
- 2.3 Waveform Modelling . . . 8
  - 2.3.1 Purpose and scope . . . 8
  - 2.3.2 Data block and Diagram . . . 8
  - 2.3.3 Mathematical Description . . . 9
- 2.4 Fitting procedure . . . 14
  - 2.4.1 Purpose and scope . . . 14
  - 2.4.2 Data block and Diagram . . . 14
  - 2.4.3 Mathematical Description . . . 14
- 2.5 Geophysical Retrievals . . . 14
  - 2.5.1 Purpose and scope . . . 14
  - 2.5.2 Data block and Diagram . . . 14
  - 2.5.3 Mathematical Description . . . 15

A Formulation differences with SAMOSA/Starlab model 17

List of Figures

2.1 Retracker flow chart. 6
2.2 Pre-processing flow chart. 7
2.3 Waveform modelling flow chart. 8
2.4 Stack generation block diagram. 10
2.5 Along-track geometry. 11
2.6 Fitting procedure block diagram. 14
2.7 Fitting procedure block diagram. 15

A.1 Comparison of $f_1(\xi)$ according to isardSAT's implementation and based on Ray *et al.* (2015) definition. 19

Nomenclature

Latin Letters

BW	Transmitted pulse bandwidth	
$B_{k,l}$	Constant term of the Taylor approximation (around $z = 0$) of the antenna pattern and surface radiation patterns' product for the l-th beam and k-th range bin	
c_0	Speed of light	m/s
end_{ns}	Last sample of the noise estimation window	
epoch_{init}	Initial epoch provided to the fitting procedure	
f_c	Carrier frequency	Hz
$f_n(\xi)$	Family of integral functions used to partially model the range-dependence of the single-look waveforms depending as a function of the dilation term g_l	
f_s	Sampling frequency	Hz
G_0	Antenna gain at boresight (maximum antenna gain)	
g_l	Dilation term in the analytical SAMOSA model	
H_{orb}	Satellite orbital height w.r.t reference ellipsoid	m
$init_{ns}$	First sample of the noise estimation window	
$I_p(\eta)$	Modified Bessel function of the first kind and order p	
k	Range bin or sample	
k_{ns}	Noise range bin or sample	
k_{offset}	Range bin offset due to the account for differences between sea height mean and the electromagnetic height bias	
l	Look, beam or Doppler index	
L_x	On-ground along-track sampling	m
L_y	On-ground across-track sampling	m
L_z	Vertical/height sampling	m
MSS	Mean-square slope	
$N_{k,\mathrm{noNaN}}$	Total number of beam samples not marked as NaN for a given range bin k	
N_{ns}	Number of samples in the noise estimation window	
N_p	Number of pulses per burst	
$P_{k,l}$	Ideal noise-free modelled power waveform for range k and beam l	
$\mathrm{PRF}_{b'}$	Pulse repetition frequency for the b'-th (burst-related) beam pointing to the surface of interest	
P_u	Fitted peak power	
R	Range distance between satellite and surface	m
R_E	Earth radius	
$S_{k,l}$	Modelled power waveform for range k and beam l	
$\tilde{S}_{k,l}$	Modelled waveform for range k and beam l after application of the mask	
$S_{k,ML}$	Multi-looked modelled waveform	
SWH	Significant wave-height	

$T_{k,l}$	Related to the linear term of the Taylor approximation (around $z = 0$) of the antenna pattern and surface radiation patterns' product for the l-th beam and k-th range bin	
$\vec{v}_s$	Satellite's velocity vector over the surface of interest	
$\vec{v}_{s,b'}$	Satellite's velocity vector for the b'-th (burst-related) beam pointing to the surface of interest	
$W_{k,l}$	Stack mask constructed from the stack mask vector contained in the L1B	
x	Along-track coordinate	m
x_p	Ground projection of the pitch angle	
y	Across-track coordinate	m
$y_{ML}(k)$	Multi-looked power waveform to be fitted	W
y_p	Ground projection of the roll angle	
z	Elevation (height) coordinate	m
ZP	Zero-padding factor in range	

Greek Letters

α_R	Orbital factor taking into account the earth curvature	
β	Pitch angle defined from nadir	rad
$\delta\theta_{look,b'}$	Look angle or Doppler resolution for the b'-th contributing beam pointing to the surface of interest	rad
δR	Range sampling including potential zero-padding	m
$\delta R_{GEOcorr}$	Geophysical correction to be applied to the retracked range	m
$\Delta\sigma^0_{atm}$	Atmospheric attenuation correction on normalized radar cross section	
γ	Roll angle defined from nadir	rad
$\eta_{th-noise}$	Threshold percentage w.r.t waveforms' peak	
$\eta_{th-peak}$	Threshold percentage w.r.t waveforms' peak	
λ	Carrier wavelength	m
$\theta_{c,b'}$	Beam angle (between vector from satellite to surface and the satellite's vector) for the b'-th contributing beam focused to the surface of interest	rad
$\theta_{Dopp,b'}$	Doppler angle (between the satellite's vector and the vector perpendicular to the nadir vector) for the b'-th contributing beam focused to the surface of interest	rad
$\theta_{look,b'}$	Look angle (between nadir and vector from satellite to surface) for the b'-th contributing beam pointing to the surface of interest	rad
$\theta_{ac,3dB}$	Across-track antenna beamwidth angle at 3dB	rad
$\theta_{al,3dB}$	Along-track antenna beamwidth angle at 3dB	rad
$\theta_{point,b'}$	Pointing angle (between antenna boresight and vector from satellite to surface) for the b'-th contributing beam focused to the surface of interest	rad
$\sigma^2_{n,l}$	Noise power for the l-th look or beam	
σ_{ac}	Standard deviation of the Gaussian-fitting to the across-track PTR	
σ_{al}	Standard deviation of the Gaussian-fitting to the along-track PTR	
σ^0	Normalized radar cross section	
σ_s	Normalized (by the vertical sampling L_z) standard deviation of the Gaussian sea height probability density function	
σ_z	Standard deviation of the Gaussian sea height probability density function	
τ_{wd}	Measured window delay	s

1 Introduction

The scope of this Algorithm Theoretical Basis Document (ATBD) is to describe all the methods and algorithms for the L2 SAR ocean processor in the frame of SCOOP project.

1.1 Document Organisation

The document is organised as:

- Section 1: Introduction.
- Section 2: SAR Ocean retracker.
- Appendix A: Formulation differences with SAMOSA/Starlab model.

1.2 Acronyms

AD applicable document

ATBD Algorithm Theoretical Basis Document

DEM Digital Elevation Model

DPM Detailed Processing Model

ESA European Space Agency

GPP Ground Prototype Processor

FFT Fast Fourier Transform

IRF Impulse Response Function

ISP Instrument Source Packet

LSE Least Square Error

LUT Look Up Table

MSS Mean-Square Slope

NaN Not a Number

NRCS Normalized Radar Cross Section

P4 Poseidon-4

PDF Probability Density Function

PRF Pulse Repetition Frequency

PTR Point Target Response

SAR Synthetic Aperture Radar

SSH Sea Surface Height

SWH Significant Wave Height

1.3 References

1.3.1 Applicable Documents

[AD1] SCOOP, "Processing Options Configuration Control Document (POCCD) D1.4," ESA, Tech. Rep., 2019, issue 1.4. (Cited on page 7.)

[AD2] ——, "Product Specification Document (PSD) - Level-1B, Level-2, RDSAR, WTC - D2.3," ESA, Tech. Rep. Proposal, March 2017, issue 1.3. (Cited on page 10.)

[AD3] E. Makhoul, F. Martin, Naeije, and D. Cotton, "SCOOP: Algorithm Theoretical Basis Document (ATBD), D1.3," ESA, Tech. Rep. SCOOP_ESA_D1.3_ATBD, 2016, issue 1.1. (Cited on pages 11 and 18.)

1.3.2 Reference Documents

[RD1] C. Ray, C. Martin-Puig, M. Clarizia, G. Ruffini, S. Dinardo, C. Gommenginger, and J. Benveniste, "SAR Altimeter Backscattered Waveform Model," *IEEE Transactions on Geoscience and Remote Sensing*, vol. 53, no. 2, pp. 911–919, 2015. [Online]. Available: http://ieeexplore.ieee.org/stamp/stamp.jsp?arnumber=6856147 (Cited on pages 5, 9, 11, 12, 18, 10, 13, 17, 19, 20, and 23.)

[RD2] C. Ray, M. Roca, C. Martin-Puig, R. Escol, and A. Garcia, "Amplitude and Dilation Compensation of the SAR Altimeter Backscattered Power," *IEEE Geoscience and Remote Sensing Letters*, vol. 12, no. 12, pp. 2473–2476, Dec 2015. (Cited on page 12.)

[RD3] J. Lillibridge, R. Scharroo, S. Abdalla, and D. Vandemark, "One- and two-dimensional wind speed models for ka-band altimetry," *Journal of Atmospheric and Oceanic Technology*, vol. 31, no. 3, pp. 630–638, 2014. [Online]. Available: https://doi.org/10.1175/JTECH-D-13-00167.1 (Cited on page 15.)

[RD4] F. V. Berghen, "CONDOR: a constrained, non-linear, derivative-free parallel optimizer for continuous, high computing load, noisy objective functions," Ph.D. dissertation, Universit Libre de Bruxelles, 2004. (Cited on pages 14 and 15.)

[RD5] G. R. Valenzuela, "Theories for the interaction of electromagnetic and oceanic waves- A review," *Boundary-Layer Meteorology*, vol. 13, pp. 61–85, Jan. 1978. (Cited on pages 12 and 19.)

2 SAR Ocean retracker

This chapter is devoted to provide a high-level description of each one of the algorithms that conform the SAR ocean retracker implemented by isardSAT, based on the model originally proposed by Ray et. al in [RD1].

2.1 General overview

The block diagram of the Level-2 processing based on the SAR ocean physical retracker is depicted in Fig. 2.1. The main steps included in this processing chain are:

1. Pre-processing
2. Stack modelling
3. Fitting procedure
4. Geophysical retrievals

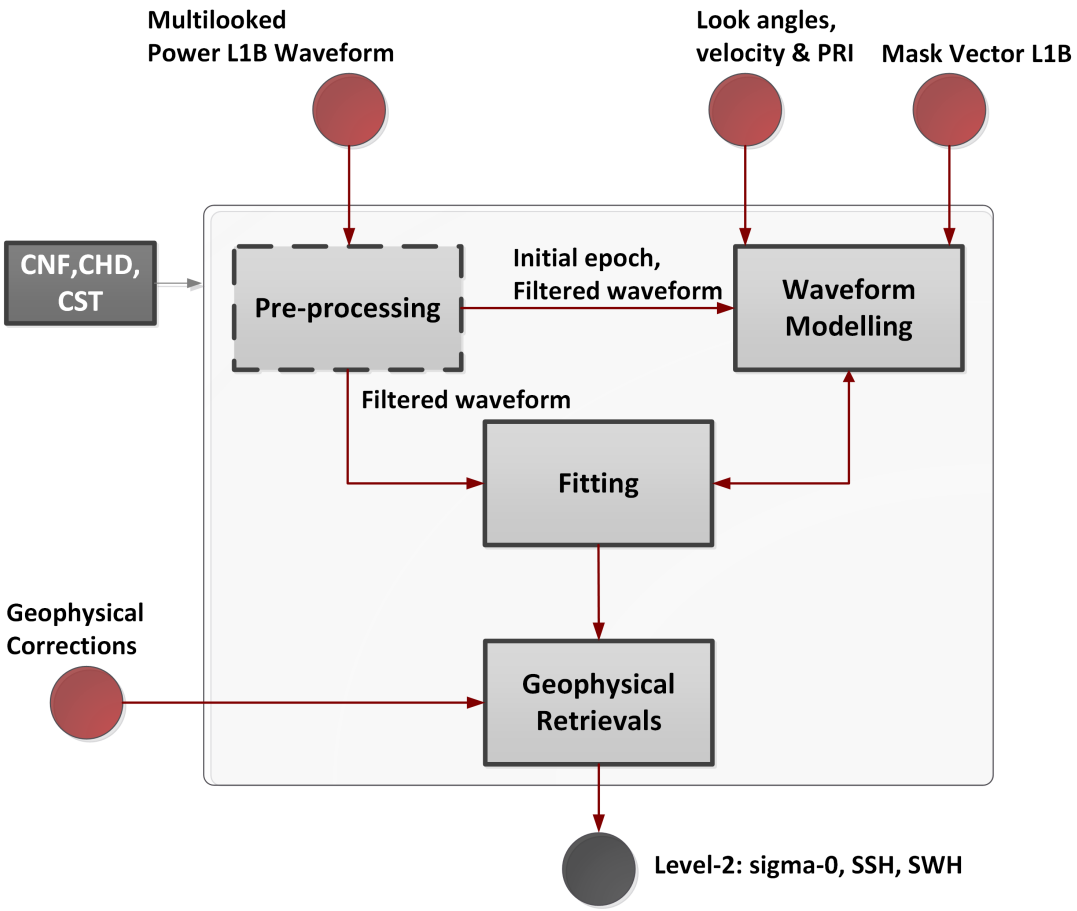

Figure 2.1: Analytical retracker block diagram (Credit: isardSAT). From now on CNF, CHD and CST refer to the configuration, characterisation and constants files provided as inputs to the L2 processor (blocks delimited by dashed lines are optionally activated).

Once the optional pre-processing stage is performed (extracting a refined initial epoch estimation for seeding the SAR ocean retracker), the fitting procedure is performed adjusting the multi-looked model waveform (obtained from the corresponding stack modelling) in a least square error minimisation procedure. Finally, the different geophysical parameters[1] are extracted, considering the application of the different geophysical corrections.

[1]The different parameters correspond to sea surface height- SSH, significant wave height - SWH and backscattering coefficient σ^0.

2.2 Pre-processing

2.2.1 Purpose and scope

This stage can be optionally activated from the configuration file (refer to [AD1] for details on the configuration parameters). A first estimation of the epoch is performed, using a simple threshold-based retracker rather than using the initial guess that can be potentially provided by the user in the configuration file. In this way, the convergence of the fitting procedure might be ensured, avoiding to lock the algorithm to a local minimum, which is not representative of the waveform being analysed.

2.2.2 Data block and Diagram

The logic of the pre-processing stage is shown in the flow chart of Fig. 2.2.

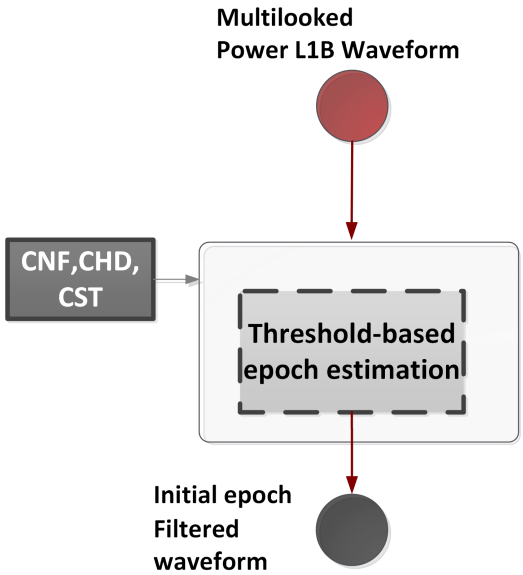

Figure 2.2: Pre-processing stage's block diagram (Credit: isardSAT): blocks delimited by dashed lines are optionally activated.

2.2.3 Mathematical Description

2.2.3.1 Threshold-based epoch estimation

For ocean-like waveforms a threshold-based retracker, where the leading edge position is estimated as a percentage of the waveform's peak, can provide a quite fair epoch guess to be used as initial value in the fitting procedure. The mathematical formulation of such retracker can be simply described as

$$\text{epoch}_{init} \mid y_{ML}\left(k = \text{epoch}_{init}\right) \leq \eta_{th-peak} \max\left(y_{ML}\left(k\right)\right) \tag{2.1}$$

where $y_{ML}\left(k\right)$ refers to the multi-looked waveform to be fitted (being k the range or bin sample); and $\eta_{th-peak}$ corresponds to the threshold percentage w.r.t the waveform's peak (typical values for ocean-like scenarios are 0.8-0.9).

2.3 Waveform Modelling

2.3.1 Purpose and scope

This processing module is in charge of generating the theoretical model of the multi-looked SAR waveform used within the fitting procedure in order to infer the different geophysical estimates (including the retracked range correction).

The key steps required to generate the multi-looked SAR waveform are:

1. Noise floor estimation
2. Stack generation
3. Stack masking
4. Multi-looking

2.3.2 Data block and Diagram

The related block diagram showing the different stages involved in the waveform modelling is represented in Fig. 2.3.

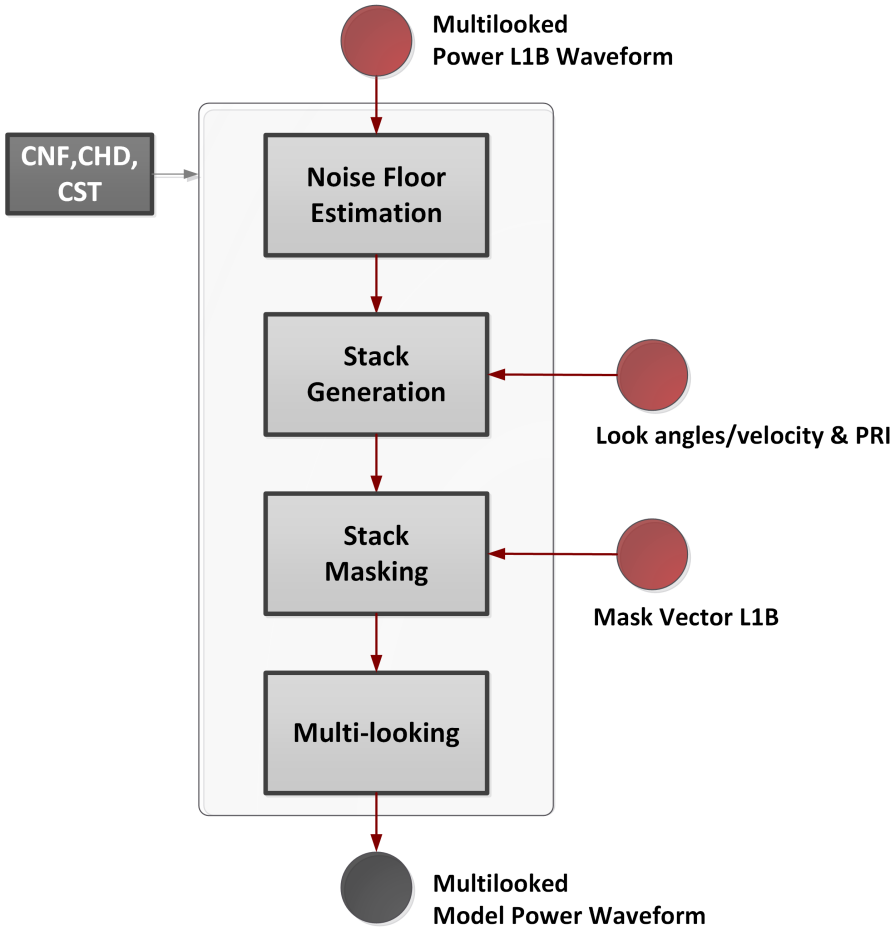

Figure 2.3: Waveform modelling block diagram (Credit: isardSAT).

2.3.3 Mathematical Description

2.3.3.1 Noise floor estimation

In order to ensure a realistic theoretical modelling of the SAR waveform the impact of thermal noise needs to be accounted for. In this way the theoretical single-look waveform can be described as:

$$S_{k,l} = P_{k,l} + \sigma^2_{n,l} \tag{2.2}$$

where $S_{k,l}$ refers to the total power echo waveform backscattered by the surface being modelled (at range bin k and look index l), $P_{k,l}$ is the only-signal modelled power echo and $\sigma^2_{n,l}$ the noise floor power for that given look index (including both thermal noise + side-lobe effects). The same noise power is considered for all the looks in the modelled stack $\sigma^2_{n,l} = \sigma^2_{n,ML}\ \forall l$, such consideration should hold as the thermal noise shall be independent and equally distributed from look to look.

A simple estimation of the noise floor can be performed using a specific window, which should be located at the beginning of the observation window, right before the leading edge and sufficiently close to it in order to incorporate the impact of the secondary lobes:

$$\sigma^2_{n,ML} = \frac{1}{N_{ns}} \sum_{k=init_{ns}}^{end_{ns}=init_{ns}+N_{ns}-1} y_{ML}\left(k\right) \tag{2.3}$$

where N_{ns} samples (starting at the $init_{ns}$ and ending at end_{ns}) of the multi-looked input power waveform $y_{ML}\left(k\right)$ are used to estimate the noise floor.

In order to define the first $init_{ns}$ and last end_{ns} samples of the noise estimation window, two different approaches can be considered (based on the configuration file settings). The first approach assumes a fixed window, exploiting the parameters defined by the user in the configuration file, such as $init_{ns}$ and size of the estimation window N_{ns}, leading to the final sample as $end_{ns} = init_{ns} + N_{ns} - 1$.

Instead of using a rough and fixed (for all waveforms) window size to estimate the noise floor, the initial $init_{ns}$ and final end_{ns} samples of the window are adaptively computed depending on each waveform being analysed, exploiting the derivative of each waveform. Then, for each waveform the estimation window can be computed as

$$k_{ns} \in [init_{ns}, end_{ns}] \mid k_{ns} \in [1, \text{epoch}_{init}) \ \& \ \frac{\partial}{\partial k} y_{ML}\left(k\right)\Big|_{k=k_{ns}} \leq \eta_{th-noise} \tag{2.4}$$

where k_{ns} refers to the samples within the noise window such that the derivative $\frac{\partial}{\partial k} y_{ML}\left(k\right)$ is below a given threshold $\eta_{th-noise}$. The critical point of this adaptive approach is precisely related to the setting/selection of the threshold.

This module can be as well de-activated during the processing. In that case an external noise estimation is ingested (based on an exhaustive estimation of the noise floor from a set of clean ocean waveforms). This would allow a proper operation of retracker even in scenarios, where land contamination of the noise section before the leading edge exists.

2.3.3.2 Stack generation

In order to obtain the multi-looked SAR waveform, the corresponding model stack should be build up from the single-look closed-form waveform solution of the retracker originally developed by Ray et al. in [RD1]. From the block diagram in Fig. 2.4 three main algorithms can be identified within the stack generation procedure:

1. Look or Doppler index generation
2. Single-look waveform modelling
3. Noise floor addition

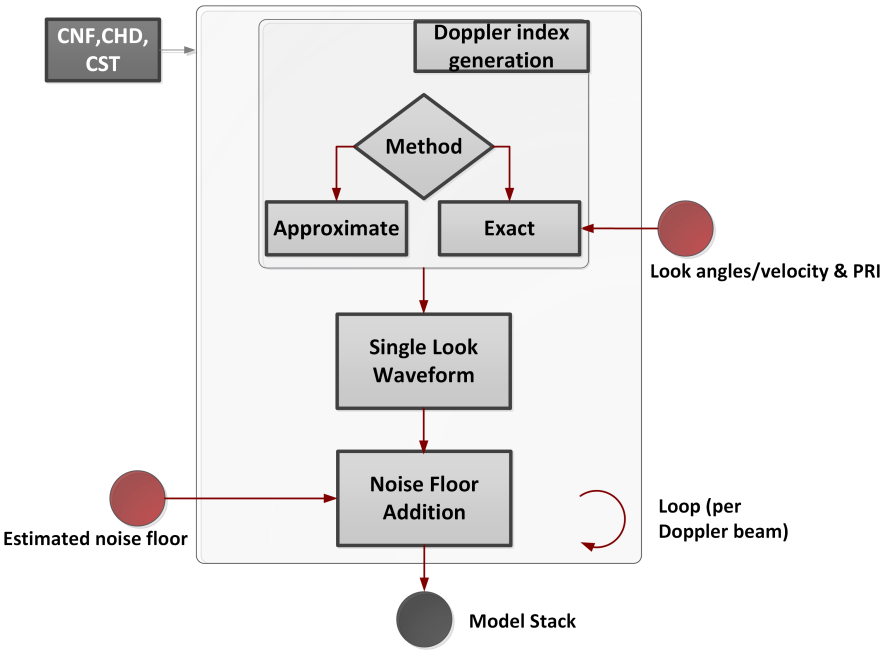

Figure 2.4: Stack generation block diagram (Credit: isardSAT).

Look indexation generation

The look or Doppler index l associated to each look in the stack being modelled [see equation (2.6)] should be properly initialised exploiting the look angle information $\theta_{look,b'}$ associated to each b' of the contributing beams (in the stack) that point to that specific surface (see Fig. 2.5[2]). Such indexation information can be computed in the Level-2 processor as

$$l = \frac{\theta_{look,b'}}{\delta\theta_{look,b'}} = \frac{\theta_{look,b'}}{\arcsin\left(\frac{\lambda \cdot \mathrm{PRF}_{b'}}{2 \cdot \|\vec{v}_{s,b'}\| \cdot N_p}\right)} \tag{2.5}$$

where $\theta_{look,b'}$ refers to the look angle for the b' contributing beam of the stack for that surface; λ corresponds to the carrier wavelength; PRF is the Pulse Repetition Frequency (PRF) associated to the b' beam (linked to a given burst[3]); $\|\vec{v}_{s,b'}\|$ is the norm of the satellite's velocity vector for the b' beam or look (which corresponds to the satellite's velocity vector for the burst related to that beam within the stack); N_p is the number of pulses.

Such an approach, from here on referred as *exact indexation method*, would increase the amount of data volume to be included at the L1B product since for each surface and each beam conforming the corresponding stack, the look angle, the satellite's velocity vector and the PRF should be annotated in the L1B product. In this sense, an *approximate* solution is considered and exploits the available information at Level-1B that can be analogously used to compute the indexation vector[4]:

- From the start and stop values of the contributing look angles θ_{look} per stack (and the total number of contributing beams per stack), the corresponding linear vector information of such angle can be constructed (each element corresponds to a given $\theta_{look,b'}$).

[2]For the flat earth geometry presented in Fig. 2.5, the look angle defined from the satellite point of view (measured from the nadir to the vector joining the satellite and the surface) is the same as the angle submitted from the surface point of view (normal of the surface to the vector joining the satellite and the surface).

[3]It corresponds to a generic formulation assuming that the contributing beams to the stack could have potential different PRFs as they are coming from different bursts, which can have different PRF as in the case of the future mission Sentinel-6.

[4]SCOOP L1B products see [AD2] incorporate the start and stop look angles contributing to the stack inherited from Sentinel-6 L1B data format since this information is not considered in the standard Sentinel-3 L1B product.

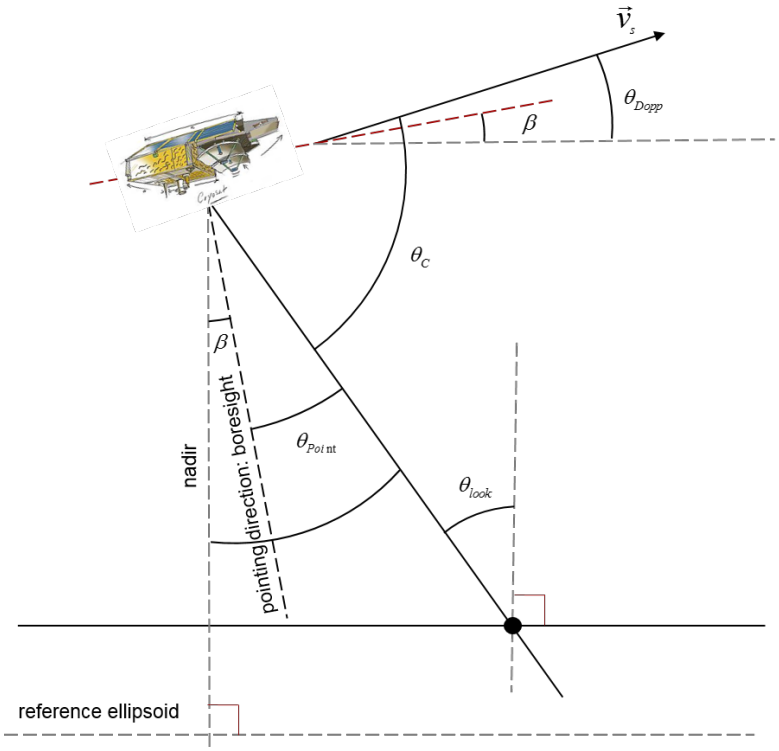

Figure 2.5: Along-track geometry: relationships between the different involved angles for a flat earth geometry (Credit: isardSAT). θ_{look} is the look angle defined by the angle from nadir to the vector joining the satellite position and the surface of interest; θ_{point} is the pointing angle defined by the angle from instrument boresight to the vector joining the satellite position and the surface of interest; θ_c corresponds to the beam angle defined between the satellite velocity vector and the vector from the satellite to that surface; θ_{Dopp} is the Doppler angle defined between the satellite's velocity vector and the vector perpendicular to the nadir; β refers to the pitch angle.

- Using the satellite's velocity $\|\vec{v}_{s,b'}\|$ and the PRF right above the surface of interest, the indexation vector can be accordingly computed as described in (2.5), exploiting the uniformly sampled vector of look angles.

Single-look waveform modelling

The original single-look model developed by Ray *et al.*, and derived for ocean-like waveforms, is being implemented in this case (assuming Gaussian ocean statistics).

Then, this algorithm is in charge of implementing the following closed-form solution of the single-look power waveform[5]:

$$P_{k,l}\left(P_u, \text{epoch}, \text{SWH}\right) = P_u \cdot B_{k,l} \cdot \sqrt{g_l\left(\text{SWH}\right)} \cdot \left[f_0\left(g_l\kappa\right) + T_{k,l} \cdot g_l\sigma_s^2 f_1\left(g_l\kappa\right)\right] \tag{2.6}$$

showing explicitly the dependency of the 3 parameters $(P_u, \text{epoch}, \text{SWH})$ used in the fitting procedure. The epoch provides an estimation of the position of the leading edge, which is used to correct the measured range (window delay) in order to provide a refined estimation of the Sea Surface Height (SSH). P_u parameter allows the retrieval of the radar backscattering coefficient or Normalized Radar Cross Section (NRCS), σ^0, once the appropriate scaling factor (computed at Level-1B) has been properly applied to the input waveform to be fitted.

As already mentioned, l denotes the look index and is related to the submitted look angle as described in

[5]Comparing this power waveform based on the original derivation in [RD1] with the one provided by Starlab in its SAMOSA model definition in SCOOP ATBD [AD3] some differences in the formulation exist. A short discussion on such issue can be found in appendix A.

the previous processing step (to construct the stack). k refers to the range bin or index and the related vector of values can be obtained as $\vec{k} = [1, \ldots, N_s]$.

The terms $B_{k,l}$ and $T_{k,l}$ incorporates the information of the **antenna pattern, antenna pointing as well as the surface scattering model** being assumed. As noted in [RD1], these components corresponds to the constant and linear term expansion of the product of the two-way antenna pattern and the surface radiation pattern NRCS.

These two terms can be expressed as follows

$$B_{k,l} = 2 \cdot e^{-\alpha_x (L_x l - x_p)^2} \cdot e^{-\alpha_\sigma (L_x l)^2} \cdot e^{-\alpha_y y_p^2} \cdot e^{-(\alpha_y + \alpha_\sigma) \cdot \left(L_y \sqrt{k}\right)^2} \cdot \cosh\left(2\alpha_y y_p L_y \sqrt{k}\right) \tag{2.7}$$

$$T_{k,l} = \frac{L_y}{\sqrt{k}} \cdot \alpha_y \cdot y_p \cdot \tanh\left(2\alpha_y y_p L_y \sqrt{k}\right) - (\alpha_y + \alpha_\sigma) \cdot L_y^2 \tag{2.8}$$

where the along- and across-track resolutions (projected on-ground) are defined as:

$$L_x = \frac{c_0 \cdot H_{orb} \cdot \mathrm{PRF}}{2 \cdot \|\vec{v}_s\| \cdot f_c \cdot N_p} \tag{2.9}$$

$$L_y = \sqrt{\frac{c_0 \cdot H_{orb}}{\alpha_R \cdot BW}} \tag{2.10}$$

being H_{orb} the orbital altitude (right above the surface); f_c the carrier frequency; $\|\vec{v}_s\|$ the norm of the satellite's velocity; N_p the number of pulses per burst; and α_R the orbital factor, i.e., $\alpha_R = 1 + \frac{H_{orb}}{R_E}$ with R_E as earth radius.

The terms $\alpha_x = \frac{8 \cdot \ln(2)}{\theta_{al,3dB}^2 \cdot H_{orb}^2}$ and $\alpha_y = \frac{8 \cdot \ln(2)}{\theta_{ac,3dB}^2 \cdot H_{orb}^2}$ in (2.7) correspond to mathematical constant group definitions, related to the ground projection of the antenna pattern beam widths in along- ($\theta_{al,3dB}$) and across-track ($\theta_{al,3dB}$) dimensions, respectively. Analogously, $x_p = -H_{orb} \cdot \beta$[6] and $y_p = H_{orb} \cdot \gamma$ refer, respectively, to the ground projection of the pitch and roll angles. The term $\alpha_\sigma = \frac{1}{H_{orb}^2 \cdot \mathrm{MSS}}$ accounts for the impact of the surface radiation pattern, under the assumption of an exponential scattering model as considered in [RD5].

Using the corresponding flag in the configuration file, it is possible to not include the impact of the antenna modulation along-track in the model (2.6). In this way the L2 modelling is aligned with the L1B processor in case the latter accounts for the compensation of the antenna pattern along-track at stack level.

An important parameter in the waveform modelling (2.6) is g_l and it can be interpreted as a **dilation term** that scales the waveform, depending only on the instrument configuration and significant wave height as defined in [RD1, RD2]:

$$g_l = \frac{1}{\sqrt{\sigma_{ac}^2 + \left(2 \cdot \sigma_{al} \cdot \frac{L_x^2}{L_y^2} \cdot l\right)^2 + \frac{\sigma_z^2}{L_z^2}}} \tag{2.11}$$

where σ_{ac} and σ_{al} correspond to the widths (standard deviations) of the Gaussian functions that approximate the Point Target Response (PTR) or Impulse Response Function (IRF) in the across- and along-track dimensions, respectively; σ_z represents the standard deviation of the Gaussian height Probability Density Function (PDF), i.e. $\sigma_z = \frac{\mathrm{SWH}}{4}$; and $L_z = \frac{c_0}{2 \cdot BW}$ is the range/height resolution, with c_0 as the light speed and BW as the transmitted pulse bandwidth.

The **range-dependent functions** $f_n(g_l \kappa)$ are modulated by the dilation term (including the beam or Doppler dependency) and can be obtained as

$$f_n(\xi) = \int_0^\infty \left(v^2 - \xi\right)^n \cdot e^{-\left(v^2 - \xi\right)^2 / 2} dv \tag{2.12}$$

[6]The minus sign definition is considered for CryoSat-2 since a positive pitch represents a nose down.

which, for order $n = 0$ and 1, can be solved using Bessel integral functions (exploiting the combination of modified Bessel functions of the first kind $I_p(\eta)$. The corresponding close form expressions are

$$f_0(\xi) = \begin{cases} 2^{1/4} \cdot \Gamma(5/4), \xi = 0 \\ \frac{\pi}{4} \cdot \sqrt{|\xi|} \cdot e^{-\frac{\xi^2}{4}} \cdot \left[I_{-1/4}\left(\frac{\xi^2}{4}\right) + \text{sign}(\xi) I_{1/4}\left(\frac{\xi^2}{4}\right) \right], \text{otherwise} \end{cases} \tag{2.13}$$

$$f_1(\xi) = \begin{cases} \frac{\Gamma(3/4)}{2 \cdot 2^{1/4}}, \xi = 0 \\ \frac{\pi}{8} \cdot (\xi)^{3/2} \cdot e^{-\xi^2/4} \cdot \left[I_{1/4}\left(\frac{\xi^2}{4}\right) - I_{-3/4}\left(\frac{\xi^2}{4}\right) + \text{sign}(\xi) \cdot \left(I_{-1/4}\left(\frac{\xi^2}{4}\right) - I_{3/4}\left(\frac{\xi^2}{4}\right) \right) \right], \text{otherwise} \end{cases} \tag{2.14}$$

To reduce the computational load of the Level-2 processor, the values of the function $f_1(\xi)$ will be tabulated, generating Look Up Tables (LUTs) to avoid calling iteratively the different Bessel functions.

Noise floor addition

Once the single-look power waveform has been generated, the estimated noise floor is added as a

$$S_{k,l}(P_u, \text{epoch}, \text{SWH}) = P_{k,l}(P_u, \text{epoch}, \text{SWH}) + \sigma^2_{n,ML} \tag{2.15}$$

Once the different look indexes have been swept, the whole modelled stack is generated.

2.3.3.3 Stack masking

To be in line with the Level-1B processing, specific masking of the modelled stack should be performed in order to mask those samples per each beam, being affected by wrapping effects due to geometry corrections, potential gaps or noisy beams.

The same mask (incorporating, among others, geometry corrections mask) applied in the Level-1B processing before multi-looking is used. For each surface a vector mask is passed to the Level-2 processor, where for each beam the first non-valid range sample or bin is indicated.

The masked stack can be modelled as

$$\tilde{S}_{k,l}(P_u, \text{epoch}, \text{SWH}) = S_{k,l}(P_u, \text{epoch}, \text{SWH}) \cdot W_{k,l} \tag{2.16}$$

where the vector mask is defined as

$$W_{k,l} = \begin{cases} 1, & \text{if } k < k_{mask,l}. \\ 0, & \text{otherwise.} \end{cases} \tag{2.17}$$

with $k_{mask,l}$ being the first range bin for the l-th beam to be masked out. It must be noted that those samples forced to zero, can be alternatively set to a Not a Number (NaN) such that they are omitted in the averaging procedure along the different beams. This is an option that has been integrated in the Level-2 processor to be aligned with the Level-1B case.

2.3.3.4 Multi-looking

After the stack has been formed, including the adequate masking, the stack is incoherently integrated (power averaging). This leads to the theoretical multi-looked waveform fed to the fitting procedure.

The multi-looking or averaging per range sample or bin k can be simply described as

$$S_{k,ML} = \frac{1}{N_{k,\text{noNaN}}} \cdot \sum_{l_{\text{noNaN}}} \tilde{S}_{k,l=l_{\text{noNaN}}},\ l_{\text{noNaN}} \in l \mid \tilde{S}_{k,l} \neq \text{NaN} \tag{2.18}$$

where in case the zero samples should not be considered in the integration, they are set to NaN values and so not included in the averaging (i.e., for each range bin only those beam samples different from NaN values are considered $N_{k,\text{noNaN}}$).

2.4 Fitting procedure

2.4.1 Purpose and scope

Based on the input waveform and the modelled one, the fitting procedure tries to converge to a solution that minimizes the error between both in a Least Square Error (LSE) basis by iteratively updating the stack model.

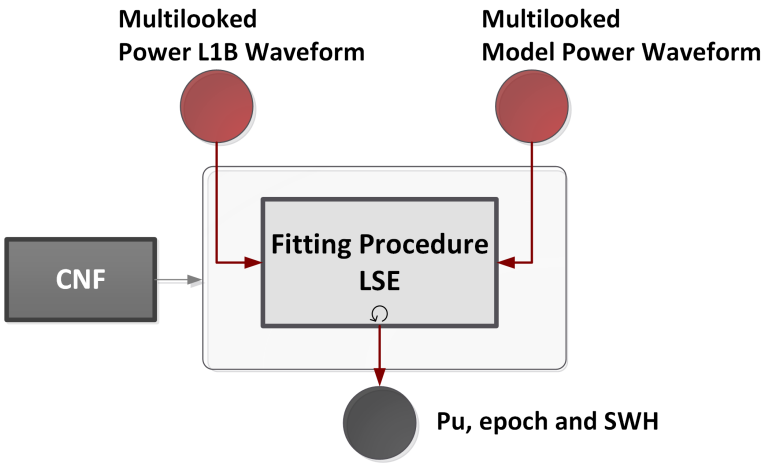

Figure 2.6: Fitting procedure block diagram (Credit: isardSAT).

2.4.2 Data block and Diagram

The flow chart of the iterative fitting method is sketched in Fig. 2.6.

2.4.3 Mathematical Description

The least-square minimisation problem can be implemented either using the *Levenberg-Marquardt* method or *trust-region-reflective* algorithm. For the latter method, the nonlinear system of equations involved in the minimisation should not be under-determined, while for the *Levenberg-Marquardt* algorithm there are no bound constrains. In fact, the *trust-region-reflective* methods are an evolution of the classical *Levenberg-Marquardt* method, some discussion on this and more specifically optimization problems can be found in [RD4].

Such fitting problem can be mathematically formulated as

$$[P_u, \text{epoch}, \text{SWH}] = \min \| S_{ML}\left(k; P_u, \text{epoch}, \text{SWH}\right) - y_{ML}\left(k\right) \| \tag{2.19}$$

being $S_{ML}\left(k; P_u, \text{epoch}, \text{SWH}\right)$ the multi-looked model waveform and $y_{ML}\left(k\right)$ the input multi-looked waveform from Level-1B product.

2.5 Geophysical Retrievals

2.5.1 Purpose and scope

This block provides the different geophysical parameters, considering the geophysical corrections to compensate for the impact of any environmental-dependent effects on the altimeter measurements.

2.5.2 Data block and Diagram

Fig. 2.7 shows the block diagram corresponding to this processing stage.

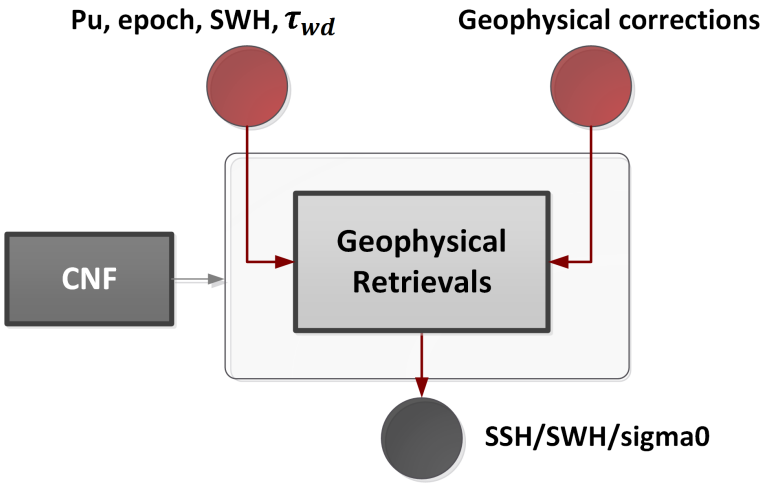

Figure 2.7: Geophysical corrections block diagram (Credit: isardSAT).

2.5.3 Mathematical Description

2.5.3.1 SSH retrieval

In order to obtain the height information of the surface above the reference ellipsoid, the satellite altitude H_{orb} and the measured range R to the surface of interest should be estimated:

$$\mathrm{SSH} = H_{orb} - (R + \Delta R_{GEOcorr}) \tag{2.20}$$

where the different geophysical corrections $\Delta R_{GEOcorr}$ are properly applied. The range is obtained from the measured window delay τ_{wd} after considering the retracker correction $\Delta\tau_{retracker}$(by means of the fitted epoch information):

$$R = c_0 \cdot \tau_{wd} + \Delta\tau_{retracker} = c_0 \cdot \tau_{wd} - (N_s/2 - \mathrm{epoch}) \cdot \delta R \tag{2.21}$$

where c_0 is the speed of light; N_s and δR correspond to the number of samples in the window and the range step (properly updated taking into account that specific zero-padding may have been considered).

2.5.3.2 σ^0 retrieval

The estimated normalized backscattering coefficient $\hat{\sigma^0}$ is obtained from the fitted power waveform amplitude

$$\hat{\sigma^0} = P_u + K_{\sigma^0} \tag{2.22}$$

where P_u represents the waveform fitted power and K_{σ^0}, a scaling factor (provided in the L1B product) to convert the received power at the flange of the antenna to σ^0 values.

The backscattered measured power and so the final estimated σ^0 are attenuated when travelling through the atmosphere, mainly due to three contributors [RD3]: attenuation due to dry atmosphere (oxygen molecules), wet atmosphere (water vapour) and cloud liquid water (water droplets or rain).

The final σ^0 is obtained as

$$\sigma^0 = \hat{\sigma^0} + \Delta\sigma^0_{atm} \tag{2.23}$$

where $\hat{\sigma^0}$ is the estimated normalized radar cross section at the output of the retracker and $\Delta\sigma^0_{atm}$ represents the atmospheric attenuation correction.

$\Delta\sigma^0_{atm}$ is obtained by spatial and temporal interpolation from the global σ^0 attenuation correction maps derived for Ku-band in [RD3], at the time and geo-location of each surface. These maps have been provided within the SCOOP project by Remko Scharroo.

2.5.3.3 Significant Wave Height (SWH) retrieval

The significant wave height is directly obtained from the output of the fitting routine.

A Formulation differences with SAMOSA/Starlab model

This appendix is devoted to provide a review on the differences between the SAR ocean retracker model used by isardSAT and the one defined by Starlab based on the SAMOSA model.

The power waveform defined in (2.6), based on Ray *et al.* formulation [RD1], leads to

$$P_{k,l} = P_u \cdot B_{k,l} \cdot \sqrt{g_l} \cdot \left[f_0\left(g_l \kappa\right) + T_{k,l} \cdot g_l \cdot \sigma_s^2 \cdot f_1\left(g_l \kappa\right) \right] \tag{A.1}$$

while in the definition of Starlab retracker [AD3] the waveform is expressed as

$$P_{k,l}^{SAMOSA} = P_u \cdot \Gamma_{k,l} \cdot \sqrt{g_l} \cdot \left[f_0\left(g_l \kappa\right) + \frac{\sigma_z}{L_\Gamma} \cdot T_{k,l}^{\text{SAMOSA}} \cdot g_l \cdot \sigma_s \cdot f_1\left(g_l \kappa\right) \right] \tag{A.2}$$

where the term $\Gamma_{k,l}$ is equivalent to $B_{k,l}$ in (A.1) and fits with the definition of the constant term of the antenna and radiation patterns product as indicated in (2.7). The term L_Γ is defined as

$$L_\Gamma = \frac{\alpha_R}{2 \cdot H_{orb} \cdot \alpha_y} \tag{A.3}$$

The definition of the term $T_{k,l}$ according to Starlab in (A.2) is

$$T_{k,l}^{\text{SAMOSA}} = \left(1 + \frac{\alpha_\sigma}{\alpha_y}\right) - \frac{y_p}{L_y \sqrt{\kappa}} \cdot \tanh\left(2 \alpha_y y_p L_y \sqrt{k}\right) \tag{A.4}$$

which can be related, except for a change of signs, to the definition of $T_{k,l}$ from (2.8) as

$$T_{k,l} = -L_y^2 \cdot \alpha_y \cdot T_{k,l}^{\text{SAMOSA}} \tag{A.5}$$

Comparing the second terms of both power waveforms (A.1) and (A.2), there are specific differences in the constant related terms:

- SAR ocean isardSAT model in (A.1), we have $\sigma_s^2 = \frac{\sigma_z^2}{L_z^2}$
- SAMOSA Starlab model in (A.2), the grouped term of constants can be written as $\frac{\sigma_z}{L_\Gamma} \cdot \sigma_s$, which is equivalent to $\frac{\sigma_z^2}{L_\Gamma \cdot L_z}$

Taking into account the definition of the terms $L_z = \frac{c_0}{2 \cdot BW}$ and $L_y = \sqrt{\frac{c_0 \cdot H_{orb}}{\alpha_R \cdot BW}}$, and using the relationship in (A.5), except for the sign, the equivalent constant factor in the second term of the power waveform in (A.1) can be arranged as

$$\frac{\sigma_z^2}{L_z^2} \cdot L_y^2 \cdot \alpha_y = \frac{\sigma_z^2}{L_z} \cdot \frac{\frac{c_0 \cdot H_{orb}}{\alpha_R \cdot BW} \cdot \alpha_y}{\frac{c_0}{2 \cdot BW}} = \frac{\sigma_z^2}{L_z} \cdot \underbrace{\frac{2 \cdot H_{orb} \cdot \alpha_y}{\alpha_R}}_{1/L_\Gamma} \tag{A.6}$$

In this way both power waveforms are equivalently defined except for the sign definition of the term $T_{k,l}$. In Figure A.1, the $f_1\left(\xi\right)$ is represented considering the integral definition (2.12) (numerically computed) against the closed-form expression using Bessel functions as per (2.14); and against the Look Up Table (LUT) implementation. The shape and values obtained are in agreement with the definition provided in Ray *et al.* (2015) [see Figure 5].

From the definition of Starlab retracker [AD3], based on SAMOSA DPM issue 2.5, the definition of the basis function is as follows

$$f_n\left(\xi\right)^{\text{SAMOSA}} = \int_0^\infty \left(-v^2 + \xi\right)^n \cdot e^{-\left(-v^2+\xi\right)^2/2} dv = (-1)^n \cdot \int_0^\infty \left(v^2 - \xi\right)^n \cdot e^{-\left(v^2-\xi\right)^2/2} dv \tag{A.7}$$

which, when compared to the definition followed by isardSAT as in (2.12), is order-dependent sign reversed.

Therefore, for the first order (n=1) base function ($f_1\left(\xi\right)$) this sign discrepancy can be absorbed in the antenna linear term $T_{k,l}^{\text{SAMOSA}}$ of the SAMOSA DPM; and so the sign definition of this term is aligned with isardSAT derivation:

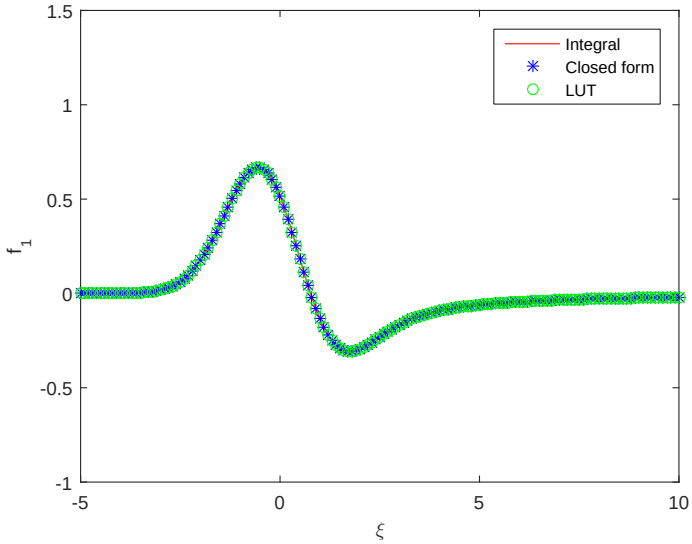

Figure A.1: Comparison of $f_1(\xi)$ according to isardSAT's implementation and based on Ray *et al.* (2015) definition.

- From isardSAT's definition of the power waveform model in equation (2.6), the $T_{k,l}$ term is expressed as follows:

$$T_{k,l} = \frac{L_y}{\sqrt{k}} \cdot \alpha_y \cdot y_p \cdot \tanh\left(2\alpha_y y_p L_y \sqrt{k}\right) - (\alpha_y + \alpha_\sigma) \cdot L_y^2 \tag{A.8}$$

- From Starlab's (SAMOSA-DPM) definition of the power waveform model (see equation below), the $T_{k,l}^{\mathrm{SAMOSA}}$ is defined as follows

$$T_{k,l}^{\mathrm{SAMOSA}} = \left(1 + \frac{\alpha_\sigma}{\alpha_y}\right) - \frac{y_p}{L_y \cdot \sqrt{k}} \cdot \tanh\left(2\alpha_y y_p L_y \sqrt{k}\right) \tag{A.9}$$